*J. Plasma Phys.* (2021), *vol*. 87, 905870408 © The Author(s), 2021. 
Published by Cambridge University Press
doi:10.1017/S0022377821000751

# Linear dispersion relation of geodesic acoustic modes driven by trapped and circulating energetic particles

**I. Chavdarovski [1],†, M. Schneller[2] and A. Biancalani [3]**

[1]Korea Institute of Fusion Energy, 34133 Daejeon, South Korea

[2]Princeton Plasma Physics Laboratory, 100 Stellarator Rd, Princeton, NJ 08540, USA

[3]Max-Planck Institute for Plasma Physics, 85748 Garching, Germany

(Received 21 February 2021; revised 18 June 2021; accepted 23 June 2021)

We derive the local dispersion relation of energetic-particle-induced geodesic acoustic modes (EGAMs) for both trapped and circulating ion beams with single pitch angle slowing-down and Maxwellian distributions, as well as a bump-on-tail distribution in tokamak plasmas. For slowing-down and Maxwellian particles, the solutions of the local dispersion relation give the spectrum, growth rate and thresholds of excitation as functions of the pitch angle, beam density and frequency of the energetic particles bounce motion. For circulating ions there is only one unstable branch with frequency below the GAM continuum and a threshold of excitation in the pitch angle, for both the slowing-down and single pitch Maxwellian distributions. Trapped particles cause no excitation of a mode for neither slowing-down nor Maxwellian ion beams, but they can excite a mode with a bump-on-tail distribution when the mean velocity of the beam is larger than the threshold and the energetic particle bounce frequency is high enough.

**Key words:** fusion plasma, plasma confinement, plasma simulation

## 1. Introduction

Geodesic acoustic modes (GAMs) (Winsor, Johnson & Dawson 1968) with frequency below that of the beta-induced Alfvén eigenmodes (BAEs) (Heidbrink *et al.* 1993; Turnbull *et al.* 1993) in the long-wavelength limit (Zonca, Chen & Santoro 1996; Zonca & Chen 2008) can be driven to instability by resonant energetic ions in tokamak plasmas (Fu 2008; Nazikian *et al.* 2008). The velocity anisotropy of the particle distribution function is essential for the excitation of these energetic-particle-driven geodesic acoustic modes (EGAMs) (Berk *et al.* 2006; Garbet *et al.* 2006; Fu 2008; Zonca, Chen & Qiu 2008). Several theoretical works have examined the linear excitation of EGAMs considering the mode interaction with the continuum and the mode conversion to short wavelength (Zonca & Chen 2008; Qiu, Zonca & Chen 2010). When the thermal ion Landau damping is taken into account (Zarzoso *et al.* 2012) the excitation of the mode is possible when the energetic particle (EP) drive exceeds the damping (Biancalani *et al.* 2017*a*). Through the ion Landau damping, EGAMs become a channel for redirection of the EP beam energy into thermal

† Email address for correspondence: chavdarovski@gmail.com

https://doi.org/10.1017/S0022377821000751 Published online by Cambridge University Press

energy of the bulk (Sasaki, Itoh & Itoh 2011; Novikau *et al.* 2020). The nonlinear dynamics and mode saturation due to redistribution of particles in velocity space (Biancalani *et al.* 2017*a*; Zarzoso *et al.* 2012) have also been studied, as well as the non-adiabatic chirping due to particle trapping (Biancalani *et al.* 2017*a*). The interaction of EGAMs with drift waves (DWs) is of particular interest since EGAMs can regulate drift wave turbulence via nonlinear interactions (Zonca & Chen 2008; Zarzoso *et al.* 2013; Dumont *et al.* 2013; Biancalani *et al.* 2017*b*; Schneller *et al.* 2016; Qiu, Chen & Zonca 2018). The nonlinear self-interaction of EGAMs has been investigated (Qiu *et al.* 2017) showing that both zero frequency zonal flow (ZFZF) and a second harmonic can be driven by finite amplitude EGAMs (Zhang *et al.* 2009; Fu 2011), opening another mechanism for EGAMs to affect the DW dynamics through the power transfer to the ZFZF (Chen, Qiu & Zonca 2014; Qiu *et al.* 2017).

In this paper we expand on the work done by Qiu *et al.* (2010), where the linear dispersion relation of EGAMs excited by a circulating slowing-down ion beam was derived. We expand the argument in two ways: (i) by including trapped energetic ions, (ii) by considering different distribution functions – single pitch slowing-down and Maxwellian, as well as bump-on-tail for trapped particles. We concentrate on modes with negligible coupling to the continuum, by having a sharp beam density profile which localizes the mode radially (Zonca & Chen 2008; Qiu *et al.* 2010; Chavdarovski *et al.* 2017; Schneller *et al.* 2017). This is analogous to the treatment of energetic particle modes (EPMs) that locally interact with the Alfvén continuum (Grad 1969; Chen & Hasegawa 1974; Hasegawa & Chen 1974; Zonca & Chen 1992; Chen 1994; Ma *et al.* 2014). The dispersion relations derived here have roots representing the GAM and EGAM as discussed in § 2, where we give a brief overview of the theoretical model and the trapped particles treatment. The solution for the trapped particles with a bump-on-tail distribution is given in § 3, while §§ 4 and 5 do the same for single pitch slowing-down and Maxwellian distributions, respectively, for both circulating and trapped particles. In § 6 numerical simulations with the gyrokinetic code GTS (Wang *et al.* 2006) show the effects of the shape of the beam on the mode structure and growth rate. The concluding remarks are given in § 7, while a detailed explanation of the derivations can be found in the Appendices A–C.

## 2. Linear dispersion relation

The model in this section follows closely the derivation of the linear dispersion relation of EGAMs for circulating energetic ions with a slowing-down distribution by Qiu *et al.* (2010). The perturbed electric field is described by the scalar potential $\delta\phi$, while the perturbed particle distribution $\delta f$ is separated into adiabatic and non-adiabatic parts ($\delta H$), where the latter is given by the linear gyrokinetic equation (Rutherford & Frieman 1968; Taylor & Hastie 1968):

$$[v_\parallel \boldsymbol{b}\cdot\boldsymbol{\nabla} - \mathrm{i}(\omega-\omega_d)]_s \delta H = \mathrm{i}(e_s/m_s)\omega f_0 \mathrm{J}_0(\lambda)\delta\phi. \tag{2.1}$$

Here, $\boldsymbol{b}\cdot\boldsymbol{\nabla} = 1/(qR_0)\partial/\partial\theta$, with $\boldsymbol{b} = \boldsymbol{B}/B$ and $q$ being the tokamak safety factor. We have assumed a small tokamak inverse aspect ratio geometry with straight field lines and $(r,\theta,\xi)$ flux coordinates, where $\theta$ and $\xi$ are the poloidal and toroidal angle-like coordinates, $r$ is the radial-like flux coordinate and $R_0$ is the major tokamak radius. The particle drift frequency is given by $\omega_d = \hat{\omega}_d \sin\theta = -k_r(v_\perp^2 + 2v_\parallel^2)/(2\Omega R_0)\sin\theta$, where $k_r \approx k_\perp$ is the radial wavenumber, $v_\perp$ and $v_\parallel$ are the particle velocities perpendicular and parallel to the magnetic field, respectively, while $\Omega = eB/mc$ is the ion gyrofrequency. In (2.1) the $\mathrm{J}(\lambda)$ term is the Bessel function of first kind, where $\lambda = k_\perp\rho_L$, with $\rho_L = v_\perp/\Omega$

https://doi.org/10.1017/S0022377821000751 Published online by Cambridge University Press

being the Larmor radius. Assuming the Larmor radius for electrons is negligible, the quasi-neutrality condition then reads (Qiu *et al.* 2010):

$$\frac{e}{T_e}(n_c+n_h)(\delta\phi-\overline{\delta\phi}) = -\frac{e}{T_e}n_c\delta\phi + \langle \mathrm{J}_0(k_\perp\rho_{L,c})\delta H_{g,c}\rangle + \left\langle \frac{e}{m}\frac{\partial F_{0h}}{\partial E}\delta\phi + \mathrm{J}_0(k_\perp\rho_{L,h})\delta H_{g,h}\right\rangle, \tag{2.2}$$

where the bar in $\overline{\delta\phi}$ implies a magnetic surfaces averaged quantity, while the indexes '$h$' and '$c$' stand for the hot and core particle populations, respectively. In (2.2) the thermal electrons are treated as adiabatic and $\delta f_e = e(\delta\phi-\overline{\delta\phi})f_0/T_e$ is used for the electron distribution function, where $T_e$ is the core electron temperature.

Adopting $\delta = n_h/n_c \ll 1$ as a smallness parameter, we assume the ordering $T_c/T_h = O(\delta)$ and $\beta_h/\beta_c \sim 1$ for the thermodynamic quantities, and treat the energetic particles non-pertubatively. Here, $\beta$ is the ratio of kinetic and magnetic pressures for each species. In order to accentuate the particle resonance we assume for the hot particles $\omega \sim \omega_{t,h}$, $\omega_{dh}/\omega \sim k_r\rho_{d,h} \sim O(\delta^{1/2})$ and $k_r\rho_{L,h} \sim O(\delta)$, where $\omega_t = v_\parallel/qR_0$ is the particle transit frequency and $\rho_{d,h}$ the radial drift, while $q \sim O(\delta^{-1/2})$. The equivalent core particle drift is $k_r\rho_{d,c} \sim O(\delta)$, while the finite Larmor effects are of higher order $k_r\rho_{L,c} \sim O(\delta^{3/2})$. Expanding all the perturbed quantities as a series of the powers of $\delta^{1/2}$, like $\delta\phi = \overline{\delta\phi} + \widetilde{\delta\phi}^{(1/2)} + \widetilde{\delta\phi}^{(1)} + \cdots$, we can solve the system of (2.1) and (2.2) order by order. It was demonstrated by Qiu *et al.* (2010) that the adopted ordering yields $\widetilde{\delta\phi}^{(1/2)} = \widetilde{\delta\phi}^{(1)} = \widetilde{\delta\phi}^{(2)} = 0$, hence to the relevant order $\delta\phi = \overline{\delta\phi} + \widehat{\delta\phi}^{(3/2)}\sin\theta$, where $\widehat{\delta\phi}^{(3/2)}$ is independent of $\theta$. The Larmor effects, which come with the Bessel functions $\mathrm{J}_0(\lambda)$ are negligible in the relevant limit for this calculation, but the drift effects should be retained. The energetic particle perturbed distribution then reduces to $\delta H_h = -(e/m)(\partial F_{0h}/\partial E)\overline{\delta\phi} + \delta H_h^{(3)}$. The first term cancels inside the angular bracket on the right-hand side of (2.2) and hence, $O(\delta^3)$ of the quasi-neutrality condition gives (see Qiu *et al.* (2010) for details)

$$-1+\omega_G^2/\omega^2 + \frac{\overline{\delta n_h}}{\overline{\delta\phi}}\frac{m\Omega_i^2}{en_ck_r^2} = 0, \tag{2.3}$$

where $\omega_G = \sqrt{7/4+\tau}\,v_{th}/R_0$ is the GAM frequency, $v_{th}$ is the core ion thermal velocity, $\tau = T_e/T_i$ and

$$\overline{\delta n_h} \simeq 2\pi B\sum_{\sigma=\pm1}\int \frac{E\,\mathrm{d}\Lambda\,\mathrm{d}E}{|v_\parallel|}\,\overline{\delta H_h^{(3)}}, \tag{2.4}$$

with $\sigma = v_\parallel/|v_\parallel|$, $\Lambda = \mu/E$ and for circulating ions (Qiu *et al.* 2010),

$$\overline{\delta H_h^{(3)}} = -\frac{\hat{\omega}_d^2\left(\frac{e}{m}\frac{\partial f_0}{\partial E}\right)}{2(\omega^2-\omega_t^2)}\overline{\delta\phi}. \tag{2.5}$$

The equivalent $\overline{\delta H_h^{(3)}}$ term for trapped particles is given in (2.8) of § 2.1.

### 2.1. *Trapped particle treatment*

To describe the trapped particles dynamics we use the deeply trapped particle approximation, where the energetic ions are conducting harmonic oscillations in

https://doi.org/10.1017/S0022377821000751 Published online by Cambridge University Press

the magnetic mirror of the tokamak field (Chavdarovski & Zonca 2009; Zonca & Chavdarovski 2009; Chavdarovski & Zonca 2014). For large aspect ratio tokamaks $\epsilon = r/R_0 \sim O(\beta^{1/2})$ the particle parallel velocity is given by $v_\parallel = \theta_b \omega_b q R_0 \cos\eta$, where $\omega_b = (\epsilon \mu B_0)^{1/2}/qR_0$ is the particle bounce frequency, $B_0$ is the magnetic field at $r = 0$, while $\theta_b^2 = 2[E - \mu B_0(1-\epsilon)]/\epsilon\mu B_0$ is the particle bounce angle, and $\eta$ is the phase angle of harmonic oscillations on the banana orbit ($\theta = \theta_b \sin\eta$). Further, $\omega_d = k_r v_d \theta_b \sin\eta$, $\hat{\omega}_d = k_r v_d$ and $v_\parallel \partial_\ell = \omega_b \partial_\eta$. We note that (2.4) is valid for trapped particles as long as we maintain the same ordering, hence $\omega \sim \omega_b$, $\hat{\omega}_d/\omega_b \sim O(\delta^{1/2})$ and $\theta_b \sim 1$. Note here that we are using the same ordering for trapped and circulating particles, assuming there is only one energetic species present at the time. If both species are to be accounted for together, they would have different orderings since they have different frequencies of motion and densities.

We pass to the banana orbit centre frame (Tsai & Chen 1993; Zonca & Chen 2016) using the substitution $\delta H = \exp(\mathrm{i}(\hat{\omega}_d/\omega_b)\theta_b \cos\eta)\delta H_b = (\Sigma_h i^h \mathrm{J}_h(\lambda_b)\mathrm{e}^{-\mathrm{i}\eta h})\delta H_b$, where $\delta H_b$ is the particle distribution function in the new frame and $\lambda_b = \theta_b(\hat{\omega}_d/\omega_b) \sim O(\delta^{1/2})$. Meanwhile, the gyrokinetic equation gives

$$[\omega_b \partial_\eta - \mathrm{i}\omega]\delta H_b = \mathrm{i}\frac{\mathrm{e}}{m}\omega \partial_E f_0 \Sigma_h (-\mathrm{i})^h \mathrm{e}^{\mathrm{i}\eta h}\mathrm{J}_0(\lambda)\mathrm{J}_h(\lambda_b)\delta\phi. \tag{2.6}$$

Due to the ordering, only $h = 0, \pm 1$ terms will contribute, i.e. only a constant term and $\omega = \pm\omega_b$ resonances appear in the final solution, thus linearizing the differential equation as

$$[\omega_b \partial_\eta - \mathrm{i}\omega]\delta H_b = \mathrm{i}\frac{\mathrm{e}}{m}\omega \partial_E f_0 \mathrm{J}_0(\lambda)[\overline{\delta\phi} + \widehat{\delta\phi}^{(3/2)}\theta_b \sin\eta][\mathrm{J}_0(\lambda_b) - 2\mathrm{i}\mathrm{J}_1(\lambda_b)\cos\eta]. \tag{2.7}$$

Dropping the higher order $\sin\eta\cos\eta$ product, it is safe to assume the solution is of a form $\delta H_b = a + b\sin\eta + c\cos\eta$, with $a$, $b$ and $c$ being constants to be determined by matching the appropriate trigonometric terms. We go back to $\delta H = (\mathrm{J}_0(\lambda_b) + \mathrm{i}\lambda_b\cos\eta)(a + b\sin\eta + c\cos\eta)$ and only keep the terms up to $O(\delta)$, which includes the finite orbit width (FOW) effects up to $\lambda_b^2$. We note again that the Larmor effects are negligible in this ordering $\mathrm{J}_0(k_\perp \rho_{Li}) = 1$, while the finite banana width gives $\mathrm{J}_0(\lambda_b) \approx 1 - \lambda_b^2/4$ and $\mathrm{J}_1(\lambda_b) \approx \lambda_b/2$. The orbit averaged $\overline{\delta H} = a\mathrm{J}_0(\lambda_b) + \mathrm{i}c\lambda_b/2$, where we used $\overline{\cos^2\eta} = 1/2$, $\overline{\cos\eta \sin\eta} = 0$, $\overline{\cos\eta} = \overline{\sin\eta} = 0$ and we took $\mathrm{J}_0^2(\lambda_b) \approx 1 - \lambda_b^2/2$ to finally get

$$\overline{\delta H} = -\frac{e}{m}\frac{\partial f_0}{\partial E}\overline{\delta\phi} - \frac{\hat{\omega}_d^2\left(\frac{e}{m}\frac{\partial f_0}{\partial E}\right)\theta_b^2}{2(\omega^2 - \omega_b^2)}\overline{\delta\phi}. \tag{2.8}$$

The first term again cancels out in the quasi-neutrality equation, while the second term is the $\overline{\delta H^{(3)}}$, which has a similar form with that of the circulating particles in (2.5), with $\omega_b$ instead of $\omega_t$, and some additional terms coming from $\theta_b^2$. Since $\theta_b \sim O(1)$, both terms are of the same order. Note here that the aforementioned approximation of $\mathrm{J}_0(\lambda_b)\mathrm{J}_1(\lambda_b)$ is overly simplified and for a better estimate, one should use a Padé approximation. However, simple numerical calculation shows that due to the shape of the distribution function, even this approximation gives very good results for values $\delta \leqslant 0.2$.

## 3. Dispersion relation for trapped particles with a bump-on-tail distribution function

The case with circulating energetic ions with a shifted Maxwellian (bump-on-tail) distribution was studied by Zarzoso *et al.* (2013). Here, we will show the

https://doi.org/10.1017/S0022377821000751 Published online by Cambridge University Press

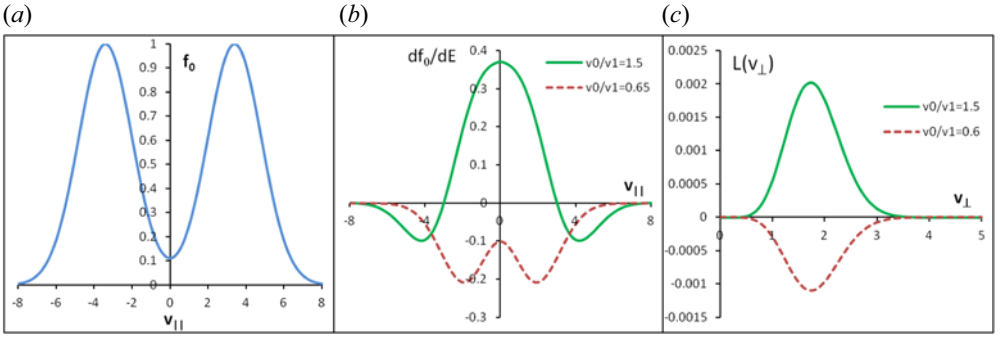


FIGURE 1. (*a*) Shifted Maxwellian distribution. (*b*) The energy derivative of the distribution as a function of $v_\parallel$. (*c*) The integrand function $L(v_\perp)$ of (3.2) as a function of $v_\perp$ and $\alpha_0 = v_0/v_1$.

derivation and results for trapped particles confined by a narrow cone in velocity space with $-v_\parallel \Delta \leqslant v_\perp \leqslant v_\parallel \Delta$, where $\Delta = 2\epsilon/(1+\epsilon)$. We consider the distribution function:

$$f_0 = c_b \exp(-(v_\perp^2/v_2^2))(\exp(-(v_\parallel - v_0)^2/v_1^2) + \exp(-(v_\parallel + v_0)^2/v_1^2)), \tag{3.1}$$

where $v_0$ is the mean parallel velocity of the beam, while the normalization factor for the trapped particle population is $c_b = n_b(r)\sqrt{\Delta^2 v_2^2 + v_1^2}/(2\pi^{3/2} v_2^3 v_1 \Delta) \exp(v_0^2/v1^2 + \Delta^2 v_2^2)$. Here, $n_b(r)$ is the beam particle density. This distribution is anisotropic in velocity space, but symmetric in $v_\parallel$ (see figure 1*a*). The derivative $\partial f_0/\partial E$ is an important factor, since it determines the slope of the distribution in energy space and hence the excitation of the mode (Fu 2008; Zarzoso *et al.* 2013). This particular distribution shows regions of positive and negative gradient depending on the beam velocity $v_0$ (figure 1*b*), making the latter a factor in the excitation of the mode. For values of $v_0/v_1$ below a certain threshold, the function is negative on the entire axis, which makes the mode stable (dashed lines in figure 1*b*).

Inserting $\partial f_0/\partial E$ in (2.4) we obtain (see Appendix A)

$$\overline{\delta n_h} = \text{const.} \int_0^\infty \frac{L(v_\perp)\, \mathrm{d}v_\perp}{v_\perp^2 - \dfrac{4\omega^2 q^2 R_0^2}{\sqrt{\Delta}}}, \tag{3.2}$$

where $L(v_\perp) = (-\exp(-(v_\perp/v_2)^2)/v_\perp)\mathrm{I}(v_\perp)$ and $I(v_\perp)$ is a fairly lengthy function given in the Appendix (A4). Even though the integrand $L(v_\perp)$ is complicated, it is a smooth function with a pronounced peak (see figure 1*c*). The figure shows that for values of $v_0$ lower than a certain threshold discussed below, the function flips the sign, which affects the possibility of excitation of the mode. The integral in (3.2) is not treatable analytically, but it can be easily integrated numerically specially in the upper half of the complex plane. For analytic purposes we will simplify the solution by Taylor expanding to the sixth order (see Appendix A) in $t = \Delta v_\perp/v_1$, around $t = 0$, which is justified for $\Delta \sim \epsilon$ and $v_2/v_1 \sim 1$. This approximation of $L(v_\perp)$ shows reasonably close behaviour to the original, and gives familiar analytic functions.

https://doi.org/10.1017/S0022377821000751 Published online by Cambridge University Press

Finally the dispersion relation of EGAMs excited by trapped particles with a bump-on-tail distribution becomes

$$0 = -1 + \frac{\omega_G^2}{\omega^2} + N_s \left[ C_6 \left( \frac{3}{4} + \frac{1}{2}\left(\frac{\omega}{\omega_b}\right)^2 + \left(\frac{\omega}{\omega_b}\right)^4 + \left(\frac{\omega}{\omega_b}\right)^5 Z\left(\frac{\omega}{\omega_b}\right)\right) + C_8 \left( \frac{15}{8} + \frac{3}{4}\left(\frac{\omega}{\omega_b}\right)^2 + \frac{1}{2}\left(\frac{\omega}{\omega_b}\right)^4 + \left(\frac{\omega}{\omega_b}\right)^6 + \left(\frac{\omega}{\omega_b}\right)^7 Z\left(\frac{\omega}{\omega_b}\right)\right)\right], \tag{3.3}$$

where the parameters are given by

$$N_s = \frac{2q^2 n_h}{n_c}\alpha_2^2(\Delta^2\alpha_2^2 + 1)^{1/2}\exp((\alpha_0^2\Delta^2\alpha_2^2)/(\Delta^2\alpha_2^2 + 1)),$$
$$C_6 = (-1 + 2\alpha_0^2)(4/3 + 16/5\Delta^2) + \Delta^4/3(-9 + 68\alpha_0^2 - 40\alpha_0^4 - 16\alpha_0^6 + 16/3\alpha_0^8) \tag{3.4}$$

and

$$C_8 = 4/15\Delta^2[(4\alpha_0^4 - 12\alpha_0^2 + 3) + \Delta^2(4\alpha_0^6 - 10\alpha_0^4 - 15\alpha_0^2 + 15/2) + 5\Delta^4(4/3\alpha_0^6 - 6\alpha_0^4 + 3\alpha_0^2 + 1/2)]. \tag{3.5}$$

Here, $\alpha_0 = v_0/v_1$, $\alpha_2 = v_2/v_1$ and $\omega_b = v_2\sqrt{\Delta}/(2qR_0)$ is the deeply trapped averaged bounce frequency for this anisotropic case, while $Z(x) = 1/\sqrt{\pi}\int_{-\infty}^{\infty} \mathrm{e}^{-y^2}/(y - x)\,\mathrm{d}y$ is the plasma dispersion function. The parameters $C_6$ and $C_8$ are functions of only $\alpha_0$ and $\Delta$. Parameter $C_6$ is the dominant one and hence a major factor in determining the growth rate. For certain values below a threshold, $C_6$ flips the sign and becomes negative. From the equation for $C_6$, we see that near $\epsilon = 0$ this threshold is simply given by $v_0/v_1 = \sqrt{2}/2$, otherwise it depends on $\Delta$ and decreases away from the axis.

It should be noted here that the bounce frequency of the trapped particles $\omega_b$ is somewhat low, so the excitation of the mode is only possible if the frequency is raised relative to the GAM frequency. This implies there can be several other thresholds for the excitation of the mode, aside from the EP density. One of them is the temperature ratio $T_h/T_c$, which is also related to $v_2$ and $\omega_b$, since for deeply trapped particles, $\omega_b \propto v_2$. A distribution which is wider in perpendicular direction raises the bounce frequency and is more likely to excite the mode, since in this way there will be a larger population with higher frequency in the tail of the distribution that can resonantly interact with the mode. This can be better seen from (3.2) where, due to the form of $L(v_\perp)$, the integral depends on the location of the resonant singularity $1/(\omega^2 - \omega_b^2)$, relative to the peak of the curve. Hence, if the resonant frequency is too low, the singularity falls to the right-hand side of the peak, while for larger frequency it is on the left side or near the peak. However, if the frequency is too high the singularity falls near $v_\perp = 0$, where $L(v_\perp)$ goes to zero.

Equation (3.3) is easily solved numerically using the Newton–Raphson method in complex space. The transcendental functions may generate multiple solutions in the negative complex plane, in which case we only deal with the most unstable branch. Figure 2 shows the frequency and normalized growth rate as functions of the particle density for different values of the beam velocity $v_0$. Increasing the EP density gives stronger excitation, while the frequency in all cases decreases as expected (Fu 2008). The threshold of $n_h$ here is relatively small due to the assumed negligible continuum and Landau damping. Some threshold of $n_h$ is expected in a realistic scenario, as is the case

https://doi.org/10.1017/S0022377821000751 Published online by Cambridge University Press

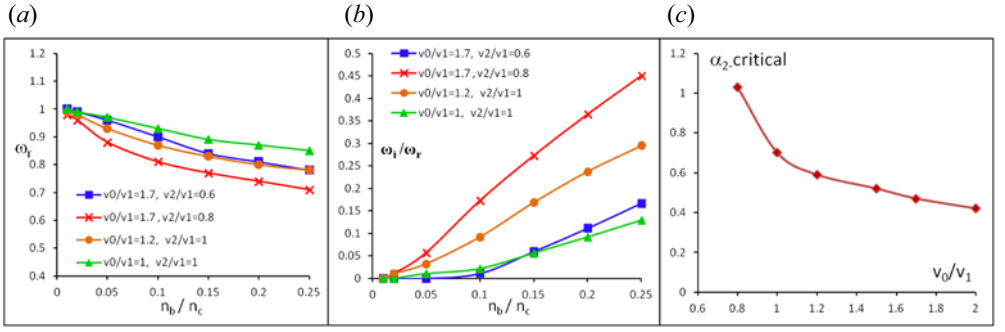


FIGURE 2. Excitation of EGAM with trapped ion beam with bump-on-tail Maxwellian distribution showing: (*a*) the real frequency normalized to $\omega_{GAM}$ and (*b*) growth rate, for different values of $\alpha_0 = v_0/v_1$ and $v_2/v_1$. (*c*) Threshold in $\alpha_2 = v_2/v_1$ as a function of $v_0/v_1$.

with all EPMs (Grad 1969; Chen 1994). In these plots we set $T_h/T_c = 8$, $q = 1.2$, $\epsilon = 0.1$ and $\tau = 1$. As discussed before larger $v_2/v_1$ and also larger beam velocity $v_0/v_1$ increase the drive of the mode. The curve with triangles ($v_0/v_1 = 1$) shows that approaching the threshold in $v_0 = \sqrt{2}/2\, v_1$ reduces the drive, while the curve with boxes, even though it has a large $\alpha_0 = 1.7$, is closer to the threshold in $v_2/v_1$ (and equivalently $\omega_b$). This threshold is shown in figure 2(*c*) for different values of $v_0/v_1$. Here, when $v_0/v_1$ approaches 0.707, $\alpha_2$ goes to infinity since this is the absolute threshold below which $L(v_\perp)$ becomes fully negative.

In all cases examined here, there is only one unstable mode and its frequency is lower than the GAM continuum, which is consistent with experimental results for circulating particles (Nazikian *et al.* 2008). In conclusion, the shifted Maxwellian provides enough controllable parameters to experimentally create the conditions for the excitation of an EGAM with trapped particles.

## 4. Slowing-down distribution

For a single pitch slowing-down distribution, $f_0 = c_0(r)\delta(\Lambda - \Lambda_0)H_E$, where $c_0(r)$ is obtained by normalization as $c_0(r) = \sqrt{2(1-\Lambda_0 B)}n_b(r)/(4\pi B \ln E_b/E_c)$ and $H_E = \Theta(1 - E/E_b)/(E^{3/2} + E_c^{3/2})$. Here, $E_c$ and $E_b$ are the energetic ion critical and birth energies, with $E_b \gg E_c$. The case for circulating particles was derived by Qiu *et al.* (2010). Here we show the result as a comparison with the other distributions and similar works (Zarzoso *et al.* 2012). Using

$$\frac{\partial}{\partial E} f_{0h} = c_0(r)\left[\delta(\Lambda - \Lambda_0)\frac{\partial}{\partial E}H_E - \frac{\Lambda}{E}H_E\frac{\partial}{\partial \Lambda}\delta(\Lambda - \Lambda_0)\right], \tag{4.1}$$

after a lengthy calculation, the EGAM dispersion relation is obtained (Qiu *et al.* 2010):

$$-1 + \frac{\omega_G^2}{\omega^2} + N_b\frac{(2-\Lambda_0 B)^2}{(1-\Lambda_0 B)^{5/2}}\left[\frac{(5\Lambda_0 B - 2)}{2(2-\Lambda_0 B)}\ln\left(1 - \frac{\omega_{ts}^2}{\omega^2}\right) + \left(\frac{1}{1-\omega_{ts}^2/\omega^2} - 1\right)\right] = 0. \tag{4.2}$$

Here, $\omega_{ts} = \sqrt{2E_b(1-\Lambda_0 B)}/(qR_0)$ is the EP transit frequency and $N_b = \sqrt{1-\Lambda_0 B}q^2 n_b(r)/4\ln(E_b/E_c)n_c$. The subscript '$s$' in the transit frequency is for the slowing-down case, where $\omega_{ts}$ is calculated at the birth energy $E_b$, while in the Maxwellian case $\omega_{tm}$ is calculated at the thermal energy $E_t = T_h/m_i$.

https://doi.org/10.1017/S0022377821000751 Published online by Cambridge University Press

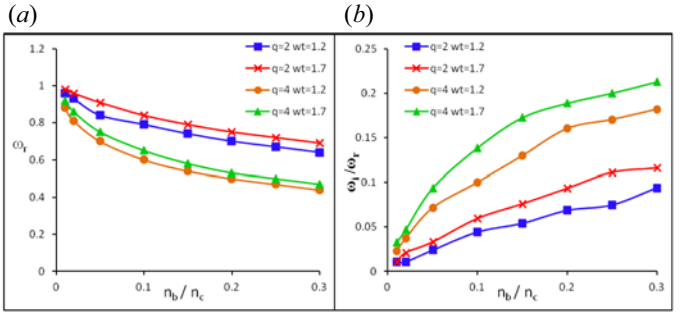


FIGURE 3. Excitation of EGAMs with circulating ion beam with slowing-down distribution showing the real frequency normalized to $\omega_{\mathrm{GAM}}$ (*a*) and growth rate (*b*).

Roughly speaking the logarithmic term represents the particle drive and shows an instability threshold $\Lambda_0 B > 2/5 = 0.4$, while the other term gives a shift from the GAM frequency. Detailed solution of the equation usually gives three different roots (similar to Fu 2008), the first one of which comes from the GAM branch $\omega = \omega_G$, and is found in (4.2) even when there is no drive ($n_h = 0$). A pair of solutions with similar frequencies, but different imaginary values, arises from the EP contribution when the value of $n_h$ is sufficiently high. The frequency and growth rates of all three branches are dependent of the EP density and resonant ion frequency, but there is only one unstable mode (Nazikian *et al.* 2008). In figure 3, we show this mode as a function of EP density for different values of $\omega_t$ and safety factor $q$, determined by the radial location of the beam.

For $\Lambda_0 B < 0.4$ or low $n_h$ the two EGAM roots become degenerate and show no excitation of a mode. The threshold $\Lambda_0 B > 0.4$ is consistent with results obtained by the gyrokinetic code GYSELA (Grandgirard *et al.* 2008; Zarzoso *et al.* 2012), where for values of $\Lambda_0 B \geqslant 0.38$ there is excitation without limitation on the critical energy. In the other region EGAMs show a threshold in $E_c$ dependent on $\Lambda$ and $E_b$ (Zarzoso *et al.* 2012). The assumption made during the derivation here was that $E_c \ll E_b$, so (4.2) can not show an $E_c$ threshold under these conditions, while finite values of $E_c$ would make (2.5) analytically non-treatable. In (4.1) the first part is always negative, while the second part can be positive or negative, hence the sign of $\partial_E f_0$ is a function of $E_c$ and this makes the excitation of the mode dependent on $E_c$.

Finally, for slowing-down trapped particles we have

$$\overline{\delta n_h} = 4AB \int (2 - \Lambda B)^2 \frac{\dfrac{\partial f_0}{\partial E} \mathrm{d}E\, \mathrm{d}\Lambda E^{5/2}}{\epsilon E \Lambda B_0 - \omega^2 q^2 R_0^2} \frac{(1 - \Lambda B)^{1/2}}{\epsilon \Lambda B_0}, \tag{4.3}$$

which leads to (see Appendix B) the dispersion relation of GAM driven by slowing-down trapped ions:

$$0 = -1 + \frac{\omega_G^2}{\omega^2} + N_b \frac{(2 - \Lambda_0 B)(9\Lambda_0 B - 10)}{(1 - \Lambda_0 B)^{1/2}} \frac{2}{(\epsilon \Lambda_0 B_0)^2} \ln\left(1 - \frac{\omega_{bs}^2}{\omega^2}\right), \tag{4.4}$$

where $\omega_{bs} = (\epsilon \Lambda_0 B E_b)^{1/2}/(qR_0)$ is the averaged ion bounce frequency. For deeply trapped particles and $\epsilon \ll 1$, the pitch angle is restricted to values $(1 - \epsilon)/(1 + \epsilon) < \Lambda_0 B < 1$. Although the secular term in (4.4) is cancelled out, the drive term is still present, but shows no excitation since the threshold in $\Lambda_0$ requires $\Lambda_0 B > 10/9$. This result is qualitatively in agreement with Zarzoso *et al.* (2012), where for high $\Lambda_0 B \sim 1$ the $E_c$ threshold becomes

https://doi.org/10.1017/S0022377821000751 Published online by Cambridge University Press

divergent, although that work considers only circulating particle dynamics, even at high $\Lambda_0$.

The dispersion relation for EGAMs excited by a not fully slowed-down energetic ion beam was derived by Cao, Qiu & Zonca (2008) in order to explain the experimental results in the Large Helical Device, where the EGAM appears before the injected neutral beam is fully slowed-down (Ido *et al.* 2015) and the birth energy is higher than the resonant considered in (4.2). The lower energy limit of not fully slowed-down particles is taken to be time variant as $E_L = E_b \mathrm{e}^{-\gamma_c t}$, where $\gamma_c \ll \omega$ is the slowing-down rate (Cao *et al.* 2008). The energetic particle square bracket term of (4.2) now has additional terms related to the lower energy limit:

$$\frac{(5\Lambda_0 B - 2)}{2(2 - \Lambda_0 B)}\left[\ln\left(1 - \frac{\omega_{ts}^2}{\omega^2}\right) - \ln\left(1 - \frac{\omega_L^2}{\omega^2}\right)\right] + \left(\frac{1}{1 - \omega_{ts}^2/\omega^2} - 1\right) - \left(\frac{1}{1 - \omega_L^2/\omega^2} - 1\right), \tag{4.5}$$

where $\omega_L = \sqrt{2E_L(1 - \Lambda_0 B)}/(qR_0)$. We note here, that the threshold related to the logarithmic term is still $\Lambda_0 B > 5/2$, and for these values the branch around $\omega_L$ is excited and can obtain a frequency larger than $\omega_G$ (see Cao *et al.* 2008 for details). However, for $\Lambda_0 B < 5/2$, where the logarithmic terms are stabilizing, the singularity in $\omega \simeq \omega_L$ can provide for a drive. Hence, in this scenario the EGAM exhibits no threshold in the pitch angle. The drive, regardless of the pitch angle, comes from the positive gradient in energy space at the lower-energy limit of the distribution function and, in that sense, more resembles the bump-on-tail drive, which gives a much bigger growth rate. In the solution for trapped particles (4.4) however, the simple singularity terms cancel out, so this mechanism does not excite EGAMs. Here, we remind the reader that the analytical model for trapped particles has several approximations, therefore we keep open the possibility of excitation with not fully slowed-down trapped particles to be demonstrated by a more rigorous calculation.

## 5. Single pitch Maxwellian distribution

The single pitch Maxwellian distribution is described by $f_{0h} = c_1(r)\delta(\Lambda - \Lambda_0)H_M$, where $c_1(r) = \sqrt{2(1 - \Lambda_0 B)}n_b(r)/(2\pi^{3/2}B)$ comes from the normalization and $H_M = 1/E_t^{3/2}\mathrm{e}^{-E/E_t}$. Using here

$$\frac{\partial}{\partial E} f_{0h} = c_1(r)\frac{1}{E_t^{5/2}}\mathrm{e}^{-E/E_t}\left[-\delta(\Lambda - \Lambda_0) - E_t\left(\frac{\Lambda}{E}\right)\frac{\partial}{\partial \Lambda}\delta(\Lambda - \Lambda_0)\right], \tag{5.1}$$

and again (2.3) and (2.4) gives the local dispersion relation for single pitch Maxwellian circulating particles (see Appendix C):

$$0 = -1 + \frac{\omega_G^2}{\omega^2} + N_m \frac{(2 - \Lambda_0 B)^2}{(1 - \Lambda_0 B)^{5/2}}(F_1 + F_2 + F_3), \tag{5.2}$$

where

$$\begin{aligned} F_1 &= -(1 - \Lambda_0 B)\left[3/4 + 1/2x^2 + x^4 + x^5 Z(x)\right], \\ F_2 &= \frac{-2 + 4\Lambda_0 B - 5/2(\Lambda_0 B)^2}{(2 - \Lambda_0 B)}\left[1/2 + x^2 + x^3 Z(x)\right], \\ F_3 &= \frac{\Lambda_0 B}{2}\left[1 + 4x^2 - 2x^4 + (5x^3 - 2x^5)Z(x)\right], \end{aligned} \tag{5.3}$$

and $N_m = \sqrt{1 - \Lambda_0 B}q^2 n_b(r)/2n_c$ with $x = \omega/\omega_{tm}$ and $\omega_{tm} = \sqrt{2E_t(1 - \Lambda_0 B)}/(qR_0)$.

https://doi.org/10.1017/S0022377821000751 Published online by Cambridge University Press

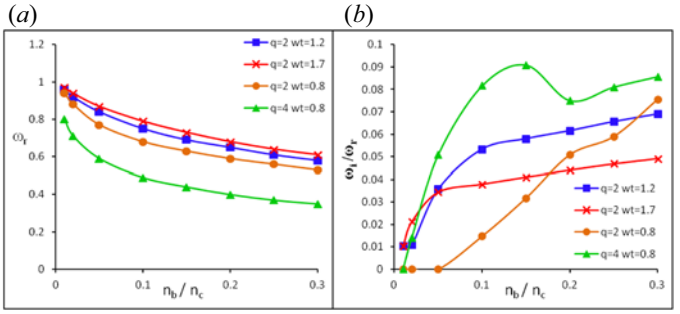


FIGURE 4. Excitation of EGAM with circulating ion beam with Maxwellian distribution showing the real frequency normalized to $\omega_{\mathrm{GAM}}$ ($a$) and growth rate ($b$).

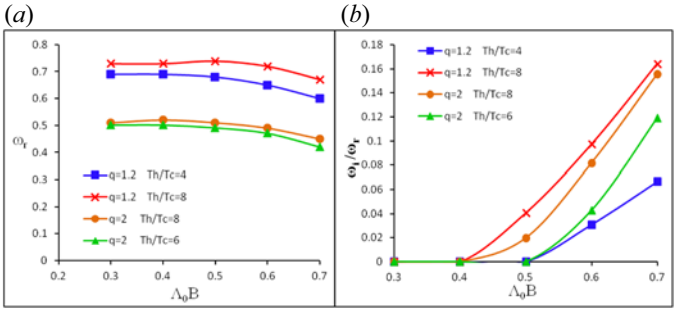


FIGURE 5. The real frequency normalized to $\omega_{\mathrm{GAM}}$ ($a$) and growth rate ($b$) versus $\Lambda_0 B$ for circulating ion beam with Maxwellian distribution showing a threshold in $\Lambda_0$.

Here again, when solving (5.2) the transcendental functions generate multiple solutions in the negative complex plane, but only one unstable branch. In figure 4 we show the real frequency and growth rate of the mode as a function of $n_b$ and $q$-safety factor. The trends are generally similar to those for slowing-down ions in figure 3 and bump-on-tail in figure 2. The threshold in EP density here is more visible, but still small. The value of the drive is also a consequence of the single pitch angle, and in a realistic case it would be smaller due to the reduced anisotropy. Even though the effect of $\Lambda_0$ on the EGAMs is not easy to interpret from (5.2), figure 5 shows there is a clear threshold in $\Lambda_0 B$ which, however, is a function of the other parameters, like $T_h$ and $q$. Careful observation of the thresholds shows that the large part of it is due to the changing of the particle bounce frequency with $\Lambda_0$.

For trapped particles with a single pitch Maxwellian distribution we have the same values for $f_{0h}$, $c_1(r)$ and $H_M$ given above. The local dispersion relation for trapped particles then reads (see Appendix C):

$$0 = -1 + \frac{\omega_G^2}{\omega^2} + N_m \frac{(2-\Lambda_0 B)(9\Lambda_0 B - 10)}{(1-\Lambda_0 B)^{1/2}} \frac{2}{(\epsilon \Lambda_0 B_0)^2} \left[1/2 + x^2 + x^3 Z(x)\right], \qquad (5.4)$$

and we have obtained the same threshold $\Lambda_0 B > 10/9$, since the function in the square brackets gives only positive values for positive imaginary frequencies. Hence, this equation too shows no excitation of EGAMs. We should mention here that the asymmetric distribution in the $\pm$ direction of $v_\parallel$ does not change the outcome of this analysis. Taking for example the work of Dannert *et al.* (2008), $f_0 \propto (\exp(v_\parallel^2/v_{T+}) + \exp(v_\parallel^2/v_{T-}))$ will

https://doi.org/10.1017/S0022377821000751 Published online by Cambridge University Press

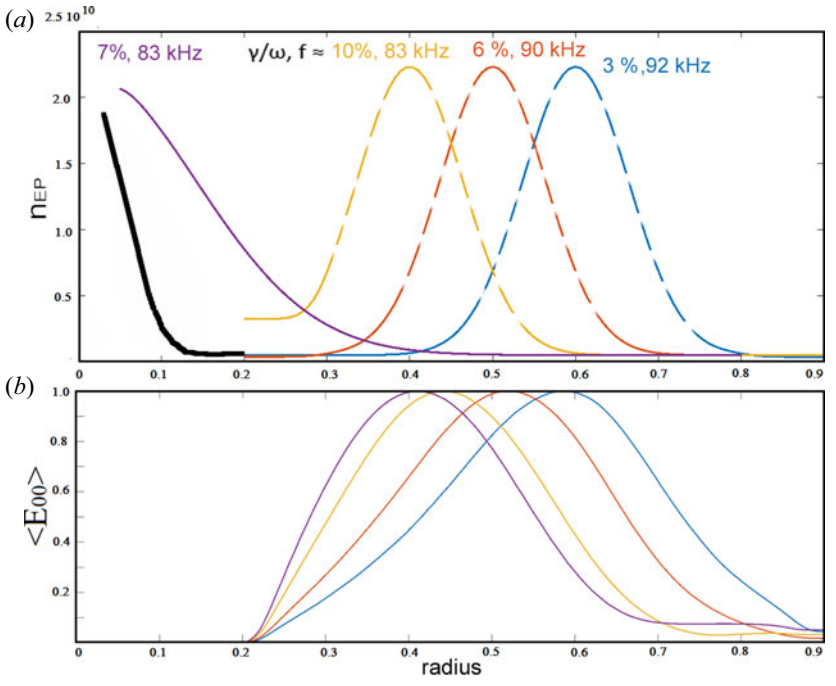


FIGURE 6. Scan of the EP density peak radial position $r/a$ ($a$) and the resulting change in the EGAM radial structure ($b$).

only change the integration in $v_\parallel$ and give $1/2[F(x_+) + F(x_-)]$, where $F(x) = 1/2 + x^2 + x^3 Z(x)$ and $x_\pm = \omega/\omega_{t\pm}$, with $\omega_{t\pm}$ having different values in different $v_\parallel$ directions. However, in both directions the sign of the function $F(x_\pm)$ is the same, which shows no solutions for trapped particles. The same parallel asymmetry conclusion can also be given for slowing-down particles. The results obtained in this work are strictly valid for deeply trapped particles, but the consistency of the results indicates that the conditions provided by the trapped ions with Maxwellian and slowing-down distributions are not favourable for the excitation of EGAMs.

## 6. Mode structure

In the previous sections we have assumed the EGAM is not coupled to the continuum, in which case the mode is localized by the Gaussian shape of the ion beam, while its radial width is determined by the FOW of the energetic particles (Fu 2008). The safety factor and beam location affect the mode frequency and drive via the values of $N_b$, $\omega_t$ and the GAM continuum. This relation is complicated since $N_b$ increases with $q$, but $\omega_t$ diminishes, while in a realistic tokamak geometry both the GAM and the bounce frequency are affected by the elongation of the magnetic flux surface. Numerical and analytical studies have examined the effects of geometry on the GAM frequency in detail (McKee *et al.* 2006; Zonca & Chen 2008; Qiu, Chen & Zonca 2009; Zhang & Lin 2010).

In figure 6 we show the excitation of EGAMs with slowing-down energetic ions using the electrostatic gyrokinetic code GTS (Wang *et al.* 2006). This code can perform global nonlinear electrostatic simulations based on a generalized gyrokinetic simulation model using a $\delta f$ particle-in-cell approach, which takes into account the comprehensive influence of many physical effects, including fully kinetic electrons and realistic geometry.

https://doi.org/10.1017/S0022377821000751 Published online by Cambridge University Press

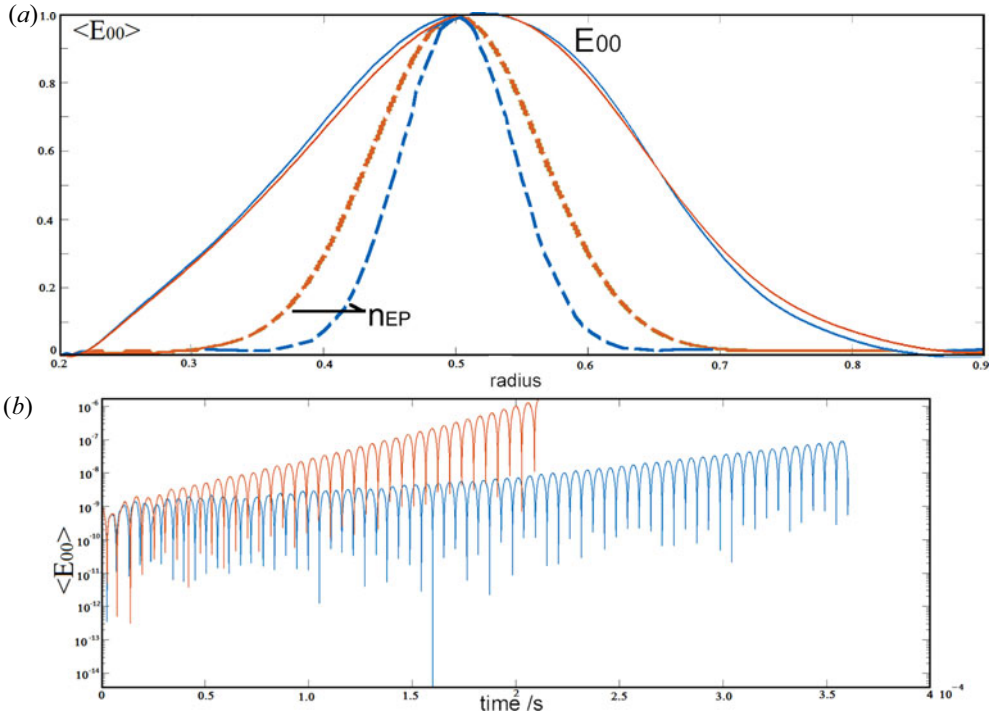


FIGURE 7. (*a*) Different radial extensions of the EP distribution function (dashed lines) and the resulting EGAM structure (solid lines), and (*b*) their growth.

Multiple ion species are implemented (background or energetic), following a distribution function of either Maxwellian, shifted-Maxwellian (bump-on-tail), bi-Maxwellian or slowing-down. Numerically, all species are treated on equal footing. In this section, the distribution in pitch angle for slowing-down ions is given by $f_0(\Lambda) = \exp(-(\Lambda - \Lambda_0)^2/(\Delta\Lambda(r))^2)$, where the width of the distribution is set to $\Delta\Lambda(r)B = 0.5$ and the peak at $\Lambda_0 B = 0.2$. The critical energy $E_c$ is above the excitation threshold, and the distribution gives (mostly) circulating particles. The mode is localized approximately around the same radial location as the beam, with small deviation which is allowed by the FOW of the energetic particles. An exception to this is when the particle beam is streaming along the axis and a mode is excited by the beam's radial tail off-axis at $x = 0.4$, where the conditions for excitation are met, which shows again that modes on the axis are more difficult to excite (Chavdarovski *et al.* 2017; Schneller *et al.* 2017). In this case, the energetic particle density around $x = 0.4$ is small, but the excitation is possible due to the FOW effects. When the energetic particles are sharply peaked on the axis we get no excitation. In figure 6 different growth rates depending on the location of the mode are obtained, which confirms that the optimal location (here $x = 0.4$) for excitation of an EGAM is away from the edge (Fu 2008).

Figure 7 shows excitation of the mode with beams of different radial widths at the same location $x = 0.5$ and with the same parameters used in figure 6. In both cases the mode structure is identical, the real frequency changes slightly, but the growth rate is strongly affected and is bigger for the wider beam. This is not a general conclusion, since there are several factors that determine the growth rate. The wider beam drives a lower frequency mode, which is related to a higher growth. This is most likely due to

https://doi.org/10.1017/S0022377821000751 Published online by Cambridge University Press

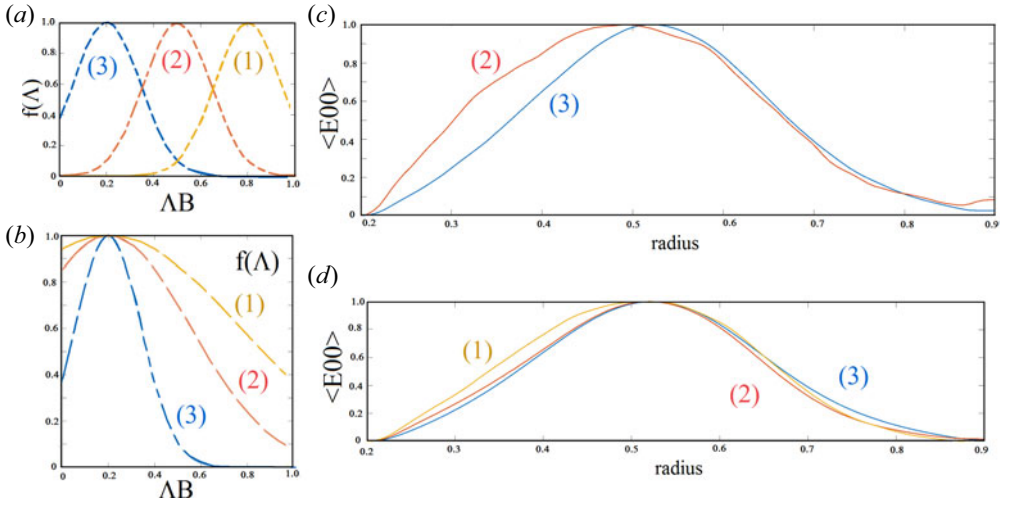


FIGURE 8. (*a*) Scan over the peak of the beam pitch angle for $\Lambda_0 B = 0.2, 0.5, 0.8$ and (*c*) resulting EGAM mode structure. (*b*) Scan over the width of the EP pitch angle distribution function: $\Delta\Lambda = 0.2, 0.5, 0.7$ and (*d*) the mode structure.

the changing of the resonant frequency with the change of the location of the energetic particles. Additionally, the wider distribution has more particles at the inside location, which shows better drive of the mode and lower frequency in figure 6. Another issue is that the relative orbit width compared with the mode structure plays an important role in determining the drive, and the orbit width is a function of the radial distribution and location.

In figure 8 the effect of the peak $\Lambda_0$ on the mode structure is shown. It should be noted that, while the analytical models take a single species, here there is a continuous distribution of particles in $\Lambda$, such that some of the particles are trapped and some circulating. When $\Lambda_0 B = 0.8$ most of the particles are trapped and show no excitation, consistent with the theoretical prediction of § 4. For lower $\Lambda_0 B$ the circulating population is dominant, while the critical energy $E_c$ is set above the excitation threshold. The particles with higher $\Lambda_0$ have larger orbit width, which gives the mode with $\Lambda_0 B = 0.5$ a slightly wider mode structure than the mode with $\Lambda_0 B = 0.2$. Figure 8(*b,d*) shows that the width of the particle distribution in energy space only slightly affects the mode shape, location and width, again due to different orbit sizes, with the wider beam (in $\Lambda$) giving a slightly wider structure.

## 7. Summary

In this work we have derived the local dispersion relations of energetic-particle-induced geodesic acoustic modes (EGAMs) for both circulating and trapped particle beams with single pitch angle slowing-down and Maxwellian distributions, as well as a bump-on-tail distribution for trapped particles. The dispersion relations for trapped particles are a novel result, as are the results for circulating particles with a single pitch Maxwellian distribution. In the case for trapped particles with a bump-on-tail distribution, the excitation of the mode shows a threshold in the density ratio of hot versus core ions. Additionally, we obtain a threshold in the mean velocity of the ion beam $v_0/v_1 = \sqrt{2}/2$, as well as a threshold in the hot ion bounce frequency determined by the $v_2/v_1$ ratio, as a function of $v_0/v_1$. The drive provided by the trapped ions with a bump-on-tail

https://doi.org/10.1017/S0022377821000751 Published online by Cambridge University Press

distribution is shown to be stronger than that for slowing-down circulating particles. For trapped particles with a slowing-down distribution the equation shows no excitation of EGAMs, which is also the case for single pitch Maxwellian, as well as Maxwellian with $\pm$ asymmetry in a $v_\parallel$ distribution.

For circulating ions with a single pitch Maxwellian distribution, we find more than the three branches that appear in the slowing-down case. However, only one of them can be unstable and that branch, identified in experiments as an EGAM, has a frequency below the GAM continuum. The dispersion relations are solved numerically for different values of the safety factor and the resonant particle frequency. The solutions show that the real frequency and growth rate of the mode are dependent of the pitch angle, the energetic particle density and their resonant frequency $\omega_t$, similar to the case for slowing-down ions. Simulations for slowing-down circulating ions with the gyrokinetic code GTS show that the structure and growth of the mode are dependent on the beam location and width, in real and energy space.

The results presented here are consistent with the experiments, but also connect well with the previously obtained analytical results.

**Acknowledgements**

Useful discussions with Z. Qiu, P. Lauber, G.Y. Fu, Z. Lu and F. Zonca are kindly acknowledged. The views and opinions expressed herein do not necessarily reflect those of the European Commission.

*Editor Francesco Califano thanks the referees for their advice in evaluating this article.*

**Funding**

This work was part of Max Planck-Princeton (MPPC) Center for Plasma Physics study 2015–2017. Work done by the coauthor A.B. has been carried out within the framework of the EUROfusion Consortium and has received funding from the Euratom research and training program 2014–2018 and 2019–2020 under grant agreement number 633053. This work was supported by R&D Program through Korean Institute of Fusion Energy (KFE) funded by the Ministry of Science and ICT of the Republic of Korea (KFE-EN2141-7).

**Declaration of interests**

The authors report no conflict of interest.

## Appendix A. Derivation for trapped particles with bump-on-tail distribution

Placing the derivative

$$\partial f_0/\partial_E = -2\frac{c_b}{v_1^2}\exp(-(v_\perp/v_2)^2)(\exp(-(v_\parallel - v_0)^2/v_1^2)(v_\parallel - v_0)/v_\parallel + \exp(-(v_\parallel + v_0)^2/v_1^2)(v_\parallel + v_0)/v_\parallel) \tag{A1}$$

in (2.4) and limiting the integral to the trapped population in velocity space, we obtain

$$\overline{\delta n_h} = \text{const.} \int_0^\infty \frac{-\exp(-(v_\perp/v_2)^2)}{v_\perp^2 - \dfrac{4\omega^2 q^2 R_0^2}{\Delta}} \frac{\mathrm{d}v_\perp}{v_\perp} \mathrm{I}(v_\perp), \tag{A2}$$

https://doi.org/10.1017/S0022377821000751 Published online by Cambridge University Press

where

$$\mathrm{I}(v_\perp) = \int_{-\Delta v_\perp}^{\Delta v_\perp} (\exp(-(v_\parallel - v_0)^2/v_1^2)(v_\parallel - v_0)/v_\parallel + \exp(-(v_\parallel + v_0)^2/v_1^2)(v_\parallel + v_0)/v_\parallel) \times (v_\perp^2 + 2v_\parallel^2)^2 \, \mathrm{d}v_\parallel. \tag{A3}$$

Integrating over $v_\parallel$ gives a rather complicated function of $v_\perp$ and $v_0$:

$$\begin{aligned}\mathrm{I}(v_\perp) = {} & P(v_\perp) v_1^2 \left( v_\perp^2(-6v_0 + 10v_0\Delta^2) + 25v_0v_1^2 + 10v_0^3 \right) \\ & + Q(v_\perp) \left( v_\perp^5(-\Delta - 4\Delta^3 + 4\Delta^5) + v_\perp^3(-6\Delta v_1^2 + 10v_1^2\Delta^3) \right. \\ & \left. + v_\perp(15v_1^4 + 10v_0^2v_1^2\Delta) \right) + R(v_\perp)\sqrt{\pi}v_1 \left( \frac{v_\perp^4}{2} + v_\perp^2(3v_1^2 + 6v_0^2) \right. \\ & \left. + \frac{15}{2}v_1^4 + 30v_1^2v_0^2 + 10v_0^4 \right).\end{aligned} \tag{A4}$$

Here, $P(v_\perp) = \exp(-(\Delta v_\perp - v_0)^2/v_1^2) - \exp(-(\Delta v_\perp + v_0)^2/v_1^2)$, $Q(v_\perp) = \exp(-(\Delta v_\perp - v_0)^2/v_1^2) + \exp(-(\Delta v_\perp + v_0)^2/v_1^2)$ and $R(v_\perp) = \mathrm{erf}(\Delta v_\perp/v_1 - v_0/v_1) + \mathrm{erf}(\Delta v_\perp/v_1 - v_0/v_1)$, where the error function is defined as $\mathrm{erf}(x) = (2/\sqrt{\pi}) \int_0^x \mathrm{e}^{-t^2} \, \mathrm{d}t$. The integrand of (A2) can be written as $L(v_\perp)/(v_\perp^2 - \omega^2 q R_0/2\sqrt{\Delta})$ where

$$L(v_\perp) = \frac{-\exp(-(v_\perp/v_2)^2)}{v_\perp} \mathrm{I}(v_\perp). \tag{A5}$$

Expanding in Taylor series to the sixth order in $t = \Delta v_\perp/v_1 < 1$,

$$\mathrm{erf}(t + v_p) + \mathrm{erf}(t - v_p) = \mathrm{e}^{-v_p^2} \left( \frac{4t}{\sqrt{\pi}} + \frac{4(-1 + 2v_p^2)t^3}{3\sqrt{\pi}} + \frac{2(3 - 12v_p^2 + 4v_p^4)t^5}{15\sqrt{\pi}} \right) \tag{A6}$$

with $v_p = v_0/v_1$, and using the usual expansions for $\exp(-(t - v_p)^2)$ and $\exp(-(t + v_p)^2)$, we get

$$\overline{\delta n_h} = \mathrm{const.} \int_0^\infty \frac{\exp(-(v_\perp/v_2)^2) v_\perp^6 (C_6 + C_8 v_\perp^2/v_1^2)}{v_\perp^2 - \dfrac{4\omega^2 q^2 R_0^2}{\Delta}} \, \mathrm{d}v_\perp. \tag{A7}$$

Here, we have omitted terms higher than $v_\perp^8$ and used the notation $C_6$ and $C_8$ for the respective constants. The integral with $C_6$ is solved using the replacement $y = v_\perp/v_2$ and

$$\mathrm{Y}_6 = \int_0^\infty \frac{\mathrm{e}^{-y^2} y^6 \, \mathrm{d}y}{y^2 - (\omega/\omega_b)^2} = \frac{\sqrt{\pi}}{2} \left[ \frac{3}{4} + \frac{1}{2} \left( \frac{\omega}{\omega_b} \right)^2 + \left( \frac{\omega}{\omega_b} \right)^4 + \left( \frac{\omega}{\omega_b} \right)^5 Z\left( \frac{\omega}{\omega_b} \right) \right], \tag{A8}$$

which is related to the plasma dispersion function $Z(x)$ (see Chavdarovski 2009, p. 105). The second integral can be obtained from $\mathrm{Y}_6$ as

$$\begin{aligned}\mathrm{Y}_8 = {} & \int_0^\infty \frac{\mathrm{e}^{-y^2} y^8 \, \mathrm{d}y}{y^2 - (\omega/\omega_b)^2} = -\int_0^\infty y^6 \mathrm{e}^{-y^2} \, \mathrm{d}x + \left( \frac{\omega}{\omega_b} \right)^2 \mathrm{Y}_6 \\ = {} & \frac{\sqrt{\pi}}{2} \left[ \frac{15}{8} + \frac{3}{4} \left( \frac{\omega}{\omega_b} \right)^2 + \frac{1}{2} \left( \frac{\omega}{\omega_b} \right)^4 + \left( \frac{\omega}{\omega_b} \right)^6 + \left( \frac{\omega}{\omega_b} \right)^7 Z\left( \frac{\omega}{\omega_b} \right) \right].\end{aligned} \tag{A9}$$

Placing these results into (2.3) gives the dispersion relation (3.3).

https://doi.org/10.1017/S0022377821000751 Published online by Cambridge University Press

## Appendix B. Derivation for slowing-down distribution

The dispersion relation follows from (2.3), where $\overline{\delta n_h}$ is obtained from the integral in (2.4):

$$\overline{\delta n_h} = 4ABc_0(r)\int (2-\Lambda B)^2 \frac{\mathrm{d}E\,\mathrm{d}\Lambda\, E^{5/2}}{\epsilon E\Lambda B_0 - \omega^2 q^2 R_0^2}\frac{(1-\Lambda B)^{1/2}}{\epsilon\Lambda B_0},$$
$$\times\left[\delta(\Lambda-\Lambda_0)\frac{\partial}{\partial E}H_E - \frac{\Lambda}{E}H_E\frac{\partial}{\partial\Lambda}\delta(\Lambda-\Lambda_0)\right], \tag{B1}$$

with $A = \pi c q^2 k_r^2 \delta\bar{\phi}/(\sqrt{2}B\Omega_i)$. The terms in the square brackets give two separate double integrals. The first one containing $\partial H_E/\partial E$ is straightforward when integrating over $\delta(\Lambda - \Lambda_0)d\Lambda$, but requires partial integration in the energy space: $\int M(E)(\partial H_E/\partial E)\,\mathrm{d}E = H_E M(E)\,|_0^\infty - \int H_E(\partial M(E)/\partial E)\,\mathrm{d}E$, where for brevity we have placed all the other quantities in the $E$-dependant $M(E)$ function. Due to the Heaviside function and $E_c \ll E_b$ we have

$$H_E M(E)\,|_0^\infty = \left[\theta(1-E/E_b)\frac{E^{5/2}}{\epsilon E\Lambda B_0 - \omega^2 q^2 R_0^2}\frac{1}{E_c^{3/2}+E^{3/2}}\right]\Bigg|_0^\infty = \frac{E^{5/2}\,|_{E=0}}{\omega^2 q^2 R_0^2 E_c^{3/2}} = 0. \tag{B2}$$

The other term of the partial integration, with the assumption $E_c \ll E \sim E_b$ and some manipulation, becomes

$$\int H_E\frac{\partial M(E)}{\partial E}\,\mathrm{d}E \propto \int_0^{E_b}\left[\frac{3/2}{\epsilon E\Lambda B_0 - \omega^2 q^2 R_0^2} - \frac{\omega^2 q^2 R_0^2}{(\epsilon E\Lambda B_0 - \omega^2 q^2 R_0^2)^2}\right]\mathrm{d}E, \tag{B3}$$

where all of the constants are extracted outside making both integrals elementary. The second part of (B1) is solved by partial integration in $d\Lambda$ as

$$\int_a^b G(E,\Lambda)\partial_\Lambda\delta(\Lambda-\Lambda_0)\,\mathrm{d}\Lambda = G(E,\Lambda)\delta(\Lambda-\Lambda_0)\,|_a^b - \int_a^b \delta(\Lambda-\Lambda_0)G_\Lambda(E,\Lambda)\,\mathrm{d}\Lambda$$
$$= -G_\Lambda(E,\Lambda_0)\theta(b-\Lambda_0)\theta(\Lambda_0-a) = -G_\Lambda(E,\Lambda_0), \tag{B4}$$

where the first term vanishes for $\Lambda_0 \in (a,b)$, with $a$ and $b$ being the limits of $\Lambda_0$, which differ for circulating and trapped particles. The derivative

$$G_\Lambda(E,\Lambda_0) = \frac{1}{\epsilon E\Lambda_0 B_0 - \omega^2 q^2 R_0^2}\frac{B(2-\Lambda_0 B)}{(1-\Lambda_0 B)^{1/2}}\left[3 - 5/2\Lambda_0 B\right]$$
$$+ \frac{\epsilon E B_0}{(\epsilon E\Lambda_0 B_0 - \omega^2 q^2 R_0^2)^2}(2-\Lambda_0 B)^2(1-\Lambda_0 B)^{1/2} \tag{B5}$$

gives the same type of integrals over $E$ as previously obtained. Hence, when all the terms are integrated and grouped together we obtain (4.4).

https://doi.org/10.1017/S0022377821000751 Published online by Cambridge University Press

## Appendix C. Derivation for Maxwellian distribution

When a single pitch Maxwellian distribution of energetic particles is used the derivative

$$\frac{\partial}{\partial E} f_{0h} = c_1(r) \frac{1}{E_t^{5/2}} \mathrm{e}^{-E/E_t} \left[ -\delta(\Lambda - \Lambda_0) - E_t \left( \frac{\Lambda}{E} \right) \frac{\partial}{\partial \Lambda} \delta(\Lambda - \Lambda_0) \right] \tag{C1}$$

again gives two integrals with delta function, where the second one additionally requires partial integration. The first integral reduces to

$$\text{const.} \cdot \int \frac{(2 - \Lambda_0 B)^2}{(1 - \Lambda_0 B)^{1/2}} \frac{E^{5/2}\, \mathrm{e}^{-E/E_t}\, \mathrm{d}E}{2E(1 - \Lambda_0 B) - \omega^2 q^2 R_0^2}, \tag{C2}$$

and the energy part is then solved using the replacement $y^2 = E/E_t$ and (A8). After the partial integration of the second term in (C1) we get two separate integrals, the first one of which has the form

$$\mathrm{Y}_4 = \int_0^\infty \frac{\mathrm{e}^{-y^2} y^4\, \mathrm{d}y}{y^2 - (\omega/\omega_t)^2} = \frac{\sqrt{\pi}}{2} \left[ \frac{1}{2} + \left( \frac{\omega}{\omega_t} \right)^2 + \left( \frac{\omega}{\omega_t} \right)^3 Z\left( \frac{\omega}{\omega_t} \right) \right] \tag{C3}$$

(see Chavdarovski 2009, p. 105), while the other

$$\mathrm{Y} = \int_0^\infty \frac{\mathrm{e}^{-y^2} y^6\, \mathrm{d}y}{(y^2 - \omega^2/\omega_t^2)^2} = -\frac{1}{2x} \frac{\partial}{\partial x} \mathrm{Y}_6, \tag{C4}$$

where $x = \omega/\omega_t$ and we have reduced Y to (A8) using the Leibnitz rule. Applying the derivative $Z_x = -(1 - xZ(x))$ inside $\partial/\partial x\, \mathrm{Y}_6$, and placing everything in (2.3), after reorganizing the terms we obtain the dispersion relation (5.2).

For trapped Maxwellian particles we can write

$$\begin{aligned} \overline{\delta n_h} = \text{const.} \int (2 - \Lambda B)^2 \frac{\mathrm{d}E\, \mathrm{d}\Lambda\, E^{5/2}}{\epsilon E \Lambda B_0 - \omega^2 q^2 R_0^2} \frac{(1 - \Lambda B)^{1/2}}{\epsilon \Lambda B_0}, \\ \times \mathrm{e}^{-E/E_t} \left[ -\delta(\Lambda - \Lambda_0) - E_t \left( \frac{\Lambda}{E} \right) \frac{\partial}{\partial \Lambda} \delta(\Lambda - \Lambda_0) \right], \end{aligned} \tag{C5}$$

where the first term is elementary, while the second term is solved as above, with an additional integral

$$\int_0^\infty \frac{\mathrm{e}^{-y^2} y^4\, \mathrm{d}y}{(y^2 - \omega^2/\omega_t^2)^2} = -\frac{1}{2x} \frac{\partial}{\partial x} \mathrm{Y}_4 \tag{C6}$$

appearing in the partial integration, which is then reduced to (C3).

## REFERENCES

BERK, H. L., BOSWELL, C. J., BORBA, D., FIGUEIREDO, A. C. A., JOHNSON, T., NAVE, M. F. F., PINCHES, S. D., SHARAPOV, S. E. & JET EFDA CONTRIBUTORS 2006 Explanation of the JET $n = 0$ chirping mode. *Nucl. Fusion* **46** (10), S888.

BIANCALANI, A., CHAVDAROVSKI, I., QIU, Z., BOTTINO, A., DEL SARTO, D., GHIZZO, A., GÜRCAN, O., MOREL, P. & NOVIKAU, I. 2017*a* Saturation of energetic-particle-driven geodesic acoustic modes due to wave particle nonlinearity. *J. Plasma Phys.* **83** (6).

https://doi.org/10.1017/S0022377821000751 Published online by Cambridge University Press

Biancalani, A., Chavdarovski, I., Qiu, Z., Di Siena, A., Gürcan, O., Jenko, F., Morel, P., Novikau, I. & Zonca, F. 2017*b* Nonlinear gyrokinetic investigation of energetic particle-driven geodesic acoustic modes. In *17th European Fusion Theory Conference, Athens, R. Greece*.

Cao, J., Qiu, Z. & Zonca, F. 2008 Fast excitation of geodesic acoustic mode by energetic particle beams. *Phys. Plasmas* **22**, 124505.

Chavdarovski, I. 2009 Kinetic theory of low frequency Alfvén waves in burning plasmas. PhD thesis. University of Tor vergata, Rome, Italy.

Chavdarovski, I., Schneller, M., Qiu, Z. & Biancalani, A. 2017 Excitation of energetic particle driven Geodesic Acoustic Modes (EGAMs) by the velocity anisotropy of ion beam with slowing down and Maxwellian distribution. In *15th IAEA Technical Meeting on Energetic Particles in Magnetic Confinement Systems, 5–8 September 2017, Princeton, NJ, USA P-3*, p. 54.

Chavdarovski, I. & Zonca, F. 2009 Effects of trapped particle dynamics on the structures of a low-frequency shear Alfvén continuous spectrum. *Plasma Phys. Control. Fusion* **51**, 115001.

Chavdarovski, I. & Zonca, F. 2014 Analytic studies of dispersive properties of shear Alfvén and acoustic wave spectra in tokamaks. *Phys. Plasmas* **21**, 052506.

Chen, L. 1994 Theory of magnetohydrodynamic instabilities excited by energetic particles in tokamaks. *Phys. Plasmas* **1**, 1519.

Chen, L. & Hasegawa, A. 1974 Plasma heating by spatial resonance of Alfvén wave. *Phys. Fluids* **17**, 1399.

Chen, L., Qiu, Z. & Zonca, F. 2014 Fine structure zonal flow excitation by beta-induced Alfvén eigenmode. *Europhys. Lett*. **107**, 15003.

Dannert, T., Günter, S., Hauff, T., Jenko, F., Lapillonne, X. & Lauber, P. 2008 Turbulent transport of beam ions. *Phys. Plasmas* **15**, 062508.

Dumont, R. J., *et al.* 2013 Interplay between fast ions and turbulence in magnetic fusion plasmas. *Plasma Phys. Control. Fusion* **55** (12), 124012.

Fu, G. Y. 2008 Energetic-particle-induced geodesic acoustic mode. *Phys. Rev. Lett*. **101**, 185002.

Fu, G. Y. 2011 On nonlinear self-interaction of geodesic acoustic mode driven by energetic particles. *J. Plasma Phys*. **77** (4), 457.

Garbet, X., Falchetto, G., Ottaviani, M., Sabot, R., Sirinelli, A. & Smolyakov, A. 2006 Coherent modes in the acoustic frequency range in tokamaks. *AIP Conf. Proc*. **871** (1), 342–349.

Grad, H. 1969 Plasmas. *Phys. Today* **22**, 34.

Grandgirard, V., *et al.* 2008 Computing ITG turbulence with a full-f semi-Lagrangian code. *Commun. Nonlinear Sci. Numer. Simul*. **13** (1), 81–87.

Hasegawa, A. & Chen, L. 1974 Plasma heating by Alfvén-wave phase mixing. *Phys. Rev. Lett*. **32**, 454.

Heidbrink, W. W., Strait, E. J., Chu, M. S. & Turnbull, A.D. 1993 Observation of beta-induced Alfvén eigenmodes in the DIII-D tokamak. *Phys. Rev. Lett*. **71**, 855.

Ido, T., *et al.* 2015 Identification of the energetic-particle driven GAM in the LHD. *Nucl. Fusion* **55**, 080324.

Ma, R., Chavdarovski, I., Ye, G. & Wang, X. 2014 Linear dispersion relation of beta-induced Alfvén eigenmodes in presence of anisotropic energetic ions. *Plasma Phys* **21**, 062120.

McKee, G. R., Gupta, D. K., Fonck, R. J., Schlossberg, D. J., Shafer, M. W. & Gohil, P. 2006 Structure and scaling properties of the geodesic acoustic mode. *Plasma Phys. Control. Fusion* **48**, S123–S136.

Nazikian, R., *et al.* 2008 Intense geodesic acousticlike modes driven by suprathermal ions in a tokamak plasma. *Phys. Rev. Lett*. **101**, 185001.

Novikau, I., *et al.* 2020 Nonlinear dynamics of energetic-particle driven geodesic acoustic modes in ASDEX upgrade. *Phys. Plasmas* **27**, 042512.

Qiu, Z., Chavdarovski, I., Biancalani, A. & Cao, J. 2017 On zero frequency zonal flow and second harmonic generation by finite amplitude energetic particle induced geodesic acoustic mode. *Phys. Plasmas* **24**, 072509.

Qiu, Z., Chen, L. & Zonca, F. 2009 Collisionless damping of short wavelength geodesic acoustic modes. *Plasma Phys. Control. Fusion* **51**, 012001.

Qiu, Z., Chen, L. & Zonca, F. 2018 Kinetic theory of geodesic acoustic modes in toroidal plasmas: a brief review. *Plasma Sci. Technol*. **20**, 094004.

https://doi.org/10.1017/S0022377821000751 Published online by Cambridge University Press

QIU, Z., ZONCA, F. & CHEN, L. 2010 Nonlocal theory of energetic-particle-induced geodesic acoustic mode. *Plasma Phys. Control. Fusion* **52**, 095003.

RUTHERFORD, P. H. & FRIEMAN, E. A. 1968 Drift instabilities in general magnetic field configurations. *Phys. Fluids* **11**, 569.

SASAKI, M., ITOH, K. & ITOH, S.-I. 2011 Energy channeling from energetic particles to bulk ions via beam-driven geodesic acoustic modes-GAM channeling. *Plasma Phys. Control. Fusion* **53** (8), 085017.

SCHNELLER, M., FU, G. Y., CHAVDAROVSKI, I., WANG, W. X., LAUBER, PH. & LU, Z. X. 2017 What shapes the radial structure of energetic particle induced geodesic acoustic modes? In *15th IAEA Technical Meeting on Energetic Particles in Magnetic Confinement Systems, 5–8 September 2017, Princeton, NJ, USA*.

SCHNELLER, M., FU, G. Y., WANG, W. X., CHAVDAROVSKI, I. & LAUBER, PH. 2016 The effect of energetic particle induced geodesic acoustic modes on microturbulence. *APS 2016* TP10. 024.

TAYLOR, J. B. & HASTIE, R. J. 1968 Stability of general plasma equilibria-I, formal theory. *Plasma Phys*. **10**, 479.

TSAI, S. T. & CHEN, L. 1993 Theory of kinetic ballooning modes excited by energetic particles in tokamaks. *Phys. Fluids* B **5**, 3284.

TURNBULL, A. D., STRAIT, E. J., HEIDBRINK, W. W., CHU, M. S., DUONG, H. H., GREENE, J. M., LAO, L. L., TAYLOR, T. S. & TOMPSON, S. J. 1993 Global Alfvén modes: theory and experiment. *Phys. Fluids* B **5**, 2546.

WANG, W. X., LIN, Z., TANG, W. M., LEE, W. W., ETHIER, S., LEWANDOWSKI, J. L. V., REWOLDT, G., HAHM, T. S. & MANICKAM, J. 2006 Gyro-kinetic simulation of global turbulent transport properties in tokamak experiments. *Phys. Plasmas* **13**, 092505.

WINSOR, N., JOHNSON, J. & DAWSON, J. M. 1968 Geodesic acoustic waves in hydromagnetic systems. *Phys. Fluids* **11**, 2448.

ZARZOSO, D., GARBET, X., SARAZIN, Y., DUMONT, R. & GRANDGIRARD, V. 2012 Fully kinetic description of the linear excitation and nonlinear saturation of fast-ion-driven geodesic acoustic mode instability. *Phys. Plasmas* **19**, 022102.

ZARZOSO, D., SARAZIN, Y., GARBET, X., STRUGAREK, A., ABITEBOUL, J., CARTIER-MICHAUD, T., DIF-PRADALIER, G., GHENDRIH, PH., GRANDGIRARD, V., LATU, G., *et al.* 2013 Impact of energetic particle driven geodesic acoustic modes on turbulence. *Phys. Rev. Lett*. **110**, 125002.

ZHANG, H., QIU, Z., CHEN, L. & LIN, Z. 2009 The importance of parallel nonlinearity in the self-interaction of geodesic acoustic mode. *Nucl. Fusion* **49**, 125009.

ZHANG, H. S. & LIN, Z. 2010 Trapped electron damping of geodesic acoustic mode. *Phys. Plasmas* **17**, 072502.

ZONCA, F. & CHAVDAROVSKI, I. 2009 Effects of trapped particle dynamics on the structures of a low-frequency shear Alfvén continuous spectrum. In *36th EPS Conference on Plasma Physics Sofia, June 29–July 3, 2009 ECA 33E*, P-1.133.

ZONCA, F. & CHEN, L. 1992 Resonant damping of toroidicity-induced shear-Alfvén eigenmodes in tokamaks. *Phys. Rev. Lett*. **68**, 592.

ZONCA, F. & CHEN, L. 2008 Radial structures and nonlinear excitation of geodesic acoustic modes. *Europhys. Lett*. **83**, 35001.

ZONCA, F. & CHEN, L. 2016 Destabilization of energetic particle modes by localized particle sources. *J. Plasma Phys*. **7** (11), 4600–4608.

ZONCA, F., CHEN, L. & QIU, Z. 2008 Kinetic theory of Geodesic Acoustic Modes: radial structures and nonlinear excitations. In *Proceedings of the 22nd International Fusion Energy Conference (Geneva, 2008)* (Vienna: IAEA) CD-ROM file TH/P 3-7.

ZONCA, F., CHEN, L. & SANTORO, R. A. 1996 Kinetic theory of low-frequency Alfvén modes in tokamaks. *Plasma Phys. Control. Fusion* **38**, 2011.

https://doi.org/10.1017/S0022377821000751 Published online by Cambridge University Press